Quantum manipulation of low-frequency fluctuators by superconducting resonator

L. Tian[1,*] and K. Jacobs[2,†]
[1]*School of Natural Sciences, University of California, Merced, California 95344, USA*
[2]*Department of Physics, University of Massachusetts at Boston, 100 Morrissey Boulevard, Boston, Massachusetts 02125, USA*
(Received 1 March 2009; published 1 April 2009)

Two-level system fluctuators in superconducting devices have demonstrated coherent coupling with superconducting qubits. Here, we show that universal quantum logic gates can be realized in these two-level systems solely by tuning a superconducting resonator in which they are imbedded. Because of the large energy separation between the fluctuators, conventional gate schemes in the cavity QED approach that are widely used for solid-state qubits cannot be directly applied to the fluctuators. We study a scheme to perform the gate operations by exploiting the controllability of the superconducting resonator with realistic parameters. Numerical simulation that takes into account the decay of the resonator mode shows that the quantum logic gates can be realized with high fidelity at moderate resonator decay rate. The quantum logic gates can also be realized between fluctuators inside different Josephson junctions that are connected by a superconducting loop. Our scheme can be applied to explore the coupling between two-level system fluctuators and superconducting resonators as well as the coherent properties of the fluctuators.

DOI: 10.1103/PhysRevB.79.144503 PACS number(s): 85.25.Cp, 03.67.Lx, 74.40.+k

I. INTRODUCTION

Spurious two-level system (TLS) fluctuators are considered a serious source of low-frequency noise in superconducting qubits,[1] and the characterization of these fluctuators in solid-state devices has a long history.[2] Most recently, coherent coupling between TLS fluctuators and a superconducting phase qubit was observed via the novel energy splittings in spectroscopic measurements.[3–5] It was shown that the TLS fluctuators have much longer decoherence times than the superconducting qubits,[6] raising the possibility of realizing quantum manipulation on these fluctuators.[7]

The key question in manipulating the TLS fluctuators is how to implement the required coherent manipulation and readout. Located sparsely inside solid-state devices, the fluctuators usually do not interact with each other, and their states are hard to control. The coupling between the fluctuators and solid-state devices provides us with a tool to achieve the quantum manipulation.[3,5] However, conventional gate schemes using cavity QED approach that are usually exploited for solid-state qubits cannot be applied to this system because of the large energy separation between the fluctuators. In this work, we will present a gate scheme that exploits the controllability of the superconducting resonator to implement high fidelity gates on the TLS fluctuators,[8–12] even when the decay of the resonator is a few megahertz. The superconducting resonator acts as a knob that controls the dynamics of individual fluctuator, as well as coupling them together. Working with practical parameters from the superconducting Josephson-junction resonator, we will design single-qubit and two-qubit quantum logic gates in the presence of resonator decay. Our scheme takes into account the full coupling Hamiltonian between the TLS fluctuators and the resonator. Readout of the fluctuators can also be performed by measuring the transmission through the resonator. This scheme can be extended to fluctuators in different Josephson junctions by connecting the junctions into the same superconducting loop due to the nonlocal nature of the microwave mode of the resonator. This work hence provides a realizable design for coherent manipulation of multiple TLS fluctuators, which is closely related to current experimental efforts in studying the fluctuators and their coupling with superconducting resonator modes.

Various superconducting resonators in the microwave regime, including superconducting transmission lines, Josephson junctions, superconducting quantum interference devices (SQUIDs), and superconducting lumped element resonators, have recently been demonstrated and have shown quantum behavior and strong coupling with superconducting qubits.[13–16] Superconducting resonators are also promising systems for studying quantum effects such as single-photon generation and lasing,[17] and one of us has shown recently that a Josephson junction can be used to probe various properties of TLS fluctuators, e.g., to resolve the mechanism that couples the fluctuators to the junction.[18] While we will focus on the Josephson-junction resonator, we want to emphasize that our results can be readily generalized to other superconducting resonators.[15,19] The paper is organized as the following. In Sec. II, we will study the coupled system of the fluctuators and a Josephson-junction resonator, including the driving on the resonator. In Sec. III, we will derive the effective Hamiltonian for the TLS fluctuators in the dispersive regime where the quantum operations are implemented. We will also derive the residual coupling between the fluctuators and the resonator in this regime. In Sec. IV, we will present detailed scheme for single-qubit and two-qubit quantum logic gates. Then, we will estimate the decoherence of the fluctuators during the gate operations in Sec. V. We will also test the fidelity of the quantum operations with numerical simulation of the full Hamiltonian, taking the resonator decay into account. In Sec. VI, we will discuss the readout of the fluctuators and the extension of gate scheme to fluctuators inside different junctions. The conclusions will be given in Sec. VII.

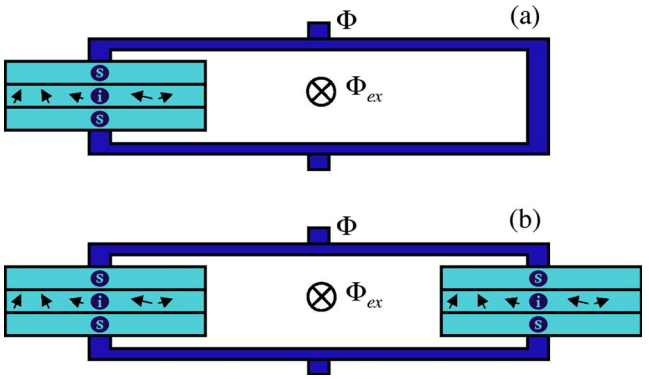

FIG. 1. (Color online) A Josephson-junction resonator containing spurious two-level system fluctuators denoted by arrows. (a) Fluctuators in a single junction and (b) fluctuators in different junctions.

II. SYSTEM

Consider the system in Fig. 1(a), where TLS fluctuators inside the amorphous layer of a Josephson junction couple with the junction resonator in an rf SQUID loop. With total capacitance C_0, Josephson energy E_J, loop inductance L, and magnetic flux $\Phi_{\rm ex}$ inside the SQUID loop, the Hamiltonian of the resonator can be written as

$$H_c = \frac{P_\Phi^2}{2C_0} - E_J \cos(2e\Phi/\hbar) + \frac{(\Phi+\Phi_{\rm ex})^2}{2L} \tag{1}$$

in terms of the phase Φ and the conjugate momentum P_Φ. This Hamiltonian can be approximated as an oscillator mode with a phase shift Φ_s from the origin,

$$H_c \approx P_\Phi^2/(2C_0) + C_0\omega_c^2(\Phi-\Phi_s)^2/2, \tag{2}$$

and the phase shift satisfies

$$\hbar\Phi_s + 2eLE_J \sin(2e\Phi_s/\hbar) = -\hbar\Phi_{\rm ex}. \tag{3}$$

The frequency of the resonator can be written as[20]

$$\omega_c = \sqrt{\frac{1}{LC_0} + \frac{4e^2E_J\cos(2e\Phi_s/\hbar)}{\hbar^2C_0}}, \tag{4}$$

which can be tuned in a large range by the magnetic flux $\Phi_{\rm ex}$. In addition, driving can be applied to the resonator by, e.g., applying an external radio-frequency current δI_c to the resonator with $\delta I_c\Phi$.

The TLS fluctuators reside inside the tunneling layer and can couple with the junction resonator by various mechanisms. For example, the coupling to the critical current of the junction takes the form $-(2e/\hbar)E_J\Phi\Sigma_n\vec{j}_n\cdot\vec{\sigma}_n$, where $\vec{j}_n$ is the polarization and magnitude of the coupling. Denoting the resonator annihilation operator by a with $\Phi-\Phi_s = \sqrt{\hbar/(2C_0\omega_c)}(a+a^\dagger)$. Let $\vec{j}_n=(j_{xn},0,0)$ for simplicity and ω_d be the driving frequency. The total Hamiltonian of the coupled system in the rotating frame can be written as

$$H_t = H_c + H_1 + H_\kappa, \tag{5}$$

$$H_c = \hbar\Delta_c a^\dagger a + \epsilon(a+a^\dagger), \tag{6}$$

$$H_1 = \sum_n [(\hbar\Delta_n/2)\sigma_{nz} + g_n(a\sigma_{n+} + a^\dagger\sigma_{n-})], \tag{7}$$

$$H_\kappa = \sum_k \hbar\omega_k a_k^\dagger a_k + c_k(a_k^\dagger a + a^\dagger a_k), \tag{8}$$

where H_c is the Hamiltonian of the driven resonator mode with the detuning $\Delta_c=\omega_c-\omega_d$ and the driving amplitude $\epsilon = \delta I_c\sqrt{\hbar/(2C_0\omega_c)}$, H_1 is the Hamiltonian of the fluctuators including the coupling between the fluctuators and the resonator mode, and H_κ is the Hamiltonian of the thermal bath connected to the resonator. Here, the index n labels different fluctuators, $\sigma_{n\alpha}$ are the Pauli operators, $\Delta_n=\omega_n-\omega_d$ is the detuning of the fluctuators, and

$$g_n = E_J j_{xn}\sqrt{\hbar/(2C_0\omega_c)}\sin(2e\Phi_s/\hbar) \tag{9}$$

is the coupling constant. Note that coupling constant for other coupling mechanisms such as dielectric coupling between the fluctuators and the resonator can be derived similarly.[18] The decay of the resonator is modeled by its coupling to a bath of modes described by the annihilation operator a_k with frequency ω_k and coupling constants c_k. The decay rate is given by $\kappa=\pi\Sigma c_k^2\delta(\omega-\omega_k)$.[21] The Hamiltonian H_t describes a typical cavity QED system between the fluctuators and the junction resonator.[22]

Note that the driving on the resonator generates a time-dependent oscillation in the phase variable with the amplitude $\delta\Phi_d=\delta I_c/C_0\omega_c^2$. To keep the nonlinear term in the Josephson energy to be small, the oscillation amplitude needs to be small, e.g., $|2e\delta\Phi_d/\hbar|<0.1$. With $1/L\sim 4e^2E_J/\hbar^2$ and typical parameters $E_J\sim 2\pi\times 100$ GHz and $C_0\sim 10^{-12}$ pF, we estimate that the driving amplitude is bounded by $\epsilon \le 2\pi\times 1$ GHz.

III. DISPERSIVE REGIME

In this work, we study the quantum logic operations in the dispersive regime where the coupling g_n is much weaker than the detuning between the fluctuators and the resonator: $g_n \ll |\Delta_{nc}|$ with $\Delta_{nc}\equiv\Delta_n-\Delta_c$. In this regime, we can apply the following unitary transformation,[8]

$$U = e^{-\epsilon(a-a^\dagger)/\Delta_c}\prod_n e^{-g_n(a^\dagger\sigma_{n-}-\sigma_{n+}a)/\Delta_{nc}}, \tag{10}$$

to the system. After the transformation, the Hamiltonian becomes $\tilde{H}_t=UH_tU^\dagger$ with $\tilde{H}_t=H_c+\tilde{H}_1+\tilde{H}_x$ to the second order of g_n/Δ_{nc}. The Hamiltonian is now divided into three parts: a Hamiltonian for the resonator H_c, an effective Hamiltonian for the fluctuators $\tilde{H}_1$, and a small residual coupling between the fluctuators and the resonator $\tilde{H}_x$.

The Hamiltonian $\tilde{H}_1$ can be written as

$$\tilde{H}_1 = \sum_n \left[\frac{\hbar\tilde{\Delta}_n}{2}\sigma_{nz} + \frac{\Omega_{nx}}{2}\sigma_{nx}\right] + H_{\rm int} + \tilde{H}_k, \tag{11}$$

$$H_{\rm int} = \sum \lambda_{mn}(\sigma_{n+}\sigma_{m-} + \sigma_{m+}\sigma_{n-})/2, \tag{12}$$

$$\tilde{H}_\kappa = \sum_{n,k} (g_n c_k/\Delta_{nc})(\sigma_{n+} a_k + a_k^\dagger \sigma_{n-}), \tag{13}$$

which includes the effective single-qubit terms, an exchangelike interaction $H_{\rm int}$, and an induced coupling to the bath modes of the resonator $\tilde{H}_\kappa$. We derive the detuning for the single qubits as

$$\tilde{\Delta}_n = \Delta_n + (g_n^2/\Delta_{nc})(1 - 2\epsilon/\Delta_c), \tag{14}$$

and the Rabi frequency as

$$\Omega_{nx} = 2\epsilon g_n/\Delta_{nc}. \tag{15}$$

The coupling constant in the exchangelike interaction can be derived as

$$\lambda_{mn} = g_m g_n(\Delta_{mc} + \Delta_{nc})/(\Delta_{mc}\Delta_{nc}). \tag{16}$$

In Sec. IV, we will study the implementation of the quantum logic gates with the Hamiltonian $\tilde{H}_1$.

The residual coupling $\tilde{H}_x$ can be written as

$$\tilde{H}_x = \sum_n \frac{g_n^2}{\Delta_{nc}} \sigma_{nz} \left[a^\dagger a + \epsilon \left(\frac{\Delta_c - 2\Delta_{nc}}{2\Delta_{nc}\Delta_c} \right) (a + a^\dagger) \right], \tag{17}$$

where the first term is the Stark shift for the resonator and the second term is a coupling to the resonator amplitude originated from the finite driving amplitude. Because of the amplitude shift in the unitary transformation in Eq. (10), the average occupation of the resonator is now zero with $\langle a^\dagger a \rangle \approx 0$. Hence, the first term has a small effect on the fluctuators during the quantum operations. The second term can induce a small modification to the coupling constant λ_{mn} in the effective interaction in Eq. (12) which will be studied in detail below.

IV. QUANTUM LOGIC GATES

Universal quantum gates can be performed by controlling the effective Hamiltonian $\tilde{H}_1$. Here, we present the scheme for the single-qubit and two-qubit gates with typical parameters from superconducting Josephson-junction resonators.

Single-qubit gates on a chosen TLS (e.g., $n=1$) can be performed by adjusting the frequency of the driving source to be close to the frequency of this TLS. By adjusting the driving amplitude and the detuning of the resonator, the effective qubit parameters $\tilde{\Delta}_1$ and Ω_{1x} can be adjusted in a wide range. For a given detuning Δ_c, one can adjust the driving amplitude ϵ in Eq. (14) to have $\tilde{\Delta}_1 = 0$ and obtain the spin-flip gate X. The gate time can be found to be $\tau_g = \pi\Delta_{nc}/2\epsilon g_n$ at the chosen ϵ. One can also adjust ϵ to have $\tilde{\Delta}_1 = \Omega_{1x}$ to implement the Hadamard gate H. Here, the driving amplitude is chosen to be

$$\epsilon = \frac{(\Delta_c\Delta_{nc} + g_n^2)\Delta_c}{2(\Delta_c + g_n)g_n}, \tag{18}$$

with the gate time $\tau_g = \pi\Delta_{nc}/2\sqrt{2}\epsilon g_n$. In Fig. 2, we plot the gate times of the Hadamard gate and spin-flip gate with the parameters $\Delta_1 = 2\pi \times 40$ MHz and $g_1 = 2\pi \times 40$ MHz. It can be shown that gate times on the order of 10 ns can be achieved.

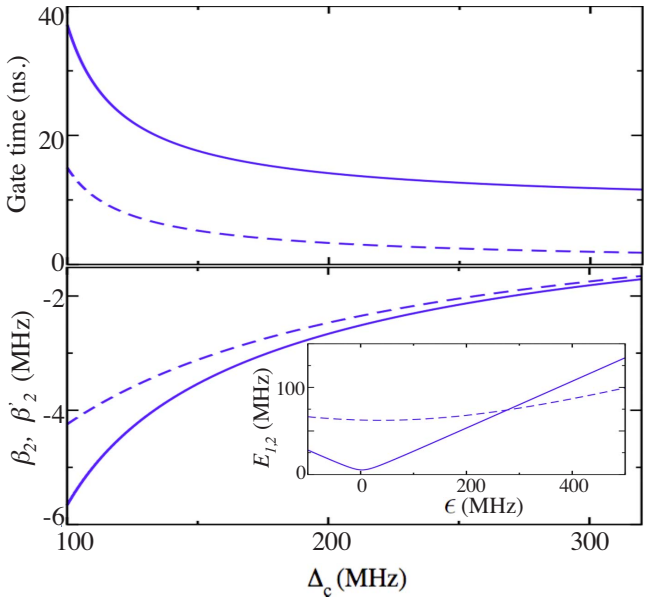

FIG. 2. (Color online) Upper plot: gate times for Hadamard gate (solid curve) and spin-flip gate (dashed curve) versus detuning Δ_c. Lower plot: effective couplings β_2 and β_2' versus Δ_c (main plot); energy E_1 (solid curve) and E_2 (dashed curve) versus ϵ at $\Delta_c = 300$ MHz (inset).

In Table I, we list two sets of gate parameters at the detunings $\Delta_c = 2\pi \times 160$ MHz for the Hadamard gate and $\Delta_c = 2\pi \times 120$ MHz for the spin-flip gate, respectively, as an example. The corresponding driving amplitudes are listed in the table. For fluctuators not involved in the gate (e.g., $n=2$), we have $\hbar\tilde{\Delta}_n \gg \Omega_{nx}$ due to the fact that the fluctuators are well separated in energy. Hence, the gate operation only induces a dynamic phase to these fluctuators. Meanwhile, the effective interaction between the fluctuators is also prevented from generating controlled phases due to the off-resonance condition $\lambda_{1n} \ll |\tilde{\Delta}_1 - \tilde{\Delta}_n|$.

Two-qubit gates can be performed via the effective exchangelike coupling in Eq. (11). This coupling can generate SWAP gate and $\sqrt{\rm SWAP}$-like controlled gates when the two qubits are near resonance with $\tilde{\Delta}_m - \tilde{\Delta}_n \sim 0$.[23] However, as noted above, the TLS fluctuators in our system are usually far off resonance from each other due to the large energy separations and are also hard to be manipulated individually. We will now show that two fluctuators can be brought into effective resonance by controlling the resonator mode, and hence high fidelity two-qubit gates can be performed. We

TABLE I. Example parameters for implementing the spin-flip gate (X) and the Hadamard gate (H).

	$\Delta_c(2\pi \times \text{MHz})$	$\epsilon(2\pi \times \text{MHz})$	$\Omega_{1x}(2\pi \times \text{MHz})$	Time (ns)
X	120	−60	60	8.3
H	160	−32	21.3	16.6

first rewrite the single TLS energy in $\tilde{H}_1$ as $\Sigma_n(E_n/2)\bar{\sigma}_{nz}$ where $E_n^2=\tilde{\Delta}_n^2+\Omega_{nx}^2$ and

$$\bar{\sigma}_{nz}=\cos\,\theta_n\sigma_{nz}+\sin\,\theta_n\sigma_{nx}, \tag{19}$$

with $\cos\,\theta_n=\tilde{\Delta}_n/E_n$ and $\sin\,\theta_n=\Omega_{nx}/E_n$. Note $\bar{\sigma}_{nx}$ and $\bar{\sigma}_{ny}$ can be defined similarly. As the driving amplitude increases, the Rabi frequency increases accordingly and the detuning $\tilde{\Delta}_n$ will be affected. As plotted in the inset of Fig. 2, a driving amplitude can be found where E_n is the same for the two fluctuators. Denoting these fluctuators as $n=1$ and $n=2$, we have $E_1=E_2$ at this point, and they are now in resonance. In the rotating frame, the effective Hamiltonian for these two fluctuators then becomes

$$H_{12}^{\rm rot}=\beta_1\bar{\sigma}_{1z}\bar{\sigma}_{2z}+\beta_2(\bar{\sigma}_{1+}\bar{\sigma}_{2-}+\bar{\sigma}_{1-}\bar{\sigma}_{2+}), \tag{20}$$

with the coefficients

$$\beta_1=(\lambda_{12}\Omega_1\Omega_2/4E_1^2), \tag{21}$$

$$\beta_2=(\lambda_{12}/4)(1+\tilde{\Delta}_1\tilde{\Delta}_2/E_1^2), \tag{22}$$

respectively. Meanwhile, at large driving amplitude with $\epsilon\sim\Delta_c$, the second term in the residual coupling $\tilde{H}_x$ in Eq. (17) induces virtual transitions between the resonator and the fluctuators, which modifies the coupling constant β_2 to become β_2'. Denoting the second term in Eq. (17) as $f_n\sigma_{nz}(a+a^\dagger)$, we can derive

$$\beta_2'=\beta_2+\frac{f_1f_2(E_1+E_2-2\Delta_c)}{2(E_1-\Delta_c)(E_2-\Delta_c)}. \tag{23}$$

In Fig. 2, we plot both the couplings β_2 and β_2' versus the resonator detuning Δ_c for comparison. A small but finite modification of the coupling coefficient can be seen. Note when $|E_{1,2}-\Delta_c|\sim\lambda_{12}$, the second term in $\tilde{H}_x$ induces real transitions between the fluctuators and the resonator, which can seriously affect the gate operations and should be avoided when designing the gates.

Two-qubit gates of the form of $S_0=\exp(-iH_{12}^{\rm rot}t)$ can now be performed in the rotating frame. A SWAP gate has the gate time $\tau_g=\pi/2|\beta_2'|$. The β_1 term in Eq. (20) contributes only phase factors in the computational basis to the gate operation. With the following parameters: $\Delta_1=0$, $\Delta_2=-2\pi\times60$ MHz, $g_1=2\pi\times40$ MHz, $g_2=2\pi\times30$ MHz, and $\Delta_c=2\pi\times300$ MHz, we find that $E_1=E_2=2\pi\times74.0$ MHz at $\epsilon=2\pi\times277.2$ MHz. Here, $\beta_2'=-2\pi\times1.8$ MHz and the SWAP gate can be performed with a gate time of $\tau_g=137.9$ ns.

We note that controlled quantum logic gates can also be performed using the Cirac-Zoller gate which was first studied in ion trap quantum computing.[24] This gate includes three steps: a swap gate between the first TLS and the resonator, a conditional phase gate between the resonator and the second TLS, and another swap gate between the first TLS and the resonator. The swap gate in the first and third steps can be implemented by choosing $\Delta_c=\Delta_1$ and $\epsilon=0$, and the gate time is $\pi/2g_1$ which is of the order of a few nanoseconds. In the conditional phase gate, the driving frequency is close to the chosen qubit but is still in the dispersive regime. The Stark shift $(g_2^2/\Delta_{2c})\sigma_{2z}a^\dagger a$ generates a conditioned phase shift on this TLS when the resonator is in state $|1\rangle$. The gate time is $t_{cg}=\pi\Delta_{2c}/2g_2^2$. At $g_2=2\pi\times30$ MHz and $\Delta_{2c}=2\pi\times120$ MHz, $t_{cg}\sim30$ ns. Note that the first TLS is subject to stronger decoherence during the swap operation due to its near-resonance coupling with the resonator, as will be discussed below.

TABLE II. Gate times τ_g, decoherence rate τ_d^{-1}, and the ratios τ_g/τ_d for single-qubit and two-qubit gates. The column labeled as "2-Qubit" is for the two-qubit gates studied in our scheme and the column labeled as "swap op." is for the swap operation in the Cirac-Zoller gate (Ref. 24).

	1-Qubit	2-Qubit	Swap op.
τ_g	$\pi\Delta_{nc}/g_n\epsilon$	$\pi/2\|\beta_2'\|$	$\pi/2g_n$
τ_d^{-1}	$g_n^2\kappa/\Delta_{nc}^2$	$g_n^2\kappa/\Delta_{nc}^2$	$\kappa/2$
τ_g/τ_d	10^{-3}	0.01	0.02

V. DECOHERENCE

The intrinsic decoherence of the TLS fluctuators is very slow and can be ignored during the gate operation. However, the coupling between the resonator and the fluctuators induces decoherence that cannot be neglected. In the dispersive regime, the decoherence rate can be calculated from the noise term $\tilde{H}_\kappa$ in Eq. (11). It can be shown that the decoherence rate is on the order of $\tau_d^{-1}\sim g_n^2\kappa/\Delta_{nc}^2$ during the quantum logic gates with $\tau_d^{-1}\ll\kappa$ in the dispersive regime. In contrast, the decoherence rate during the swap operation in the Cirac-Zoller gate is $\tau_d^{-1}\sim\kappa/2$ which is much faster than the decoherence rate in the dispersive regime. In Table II, we list the gate times, the decoherence rates, and the ratios of gate times to decoherence times for the gates discussed above at $\kappa=4$ MHz.

One can estimate the gate fidelity approximately as

$$F=e^{-\tau_g/\tau_d}\approx1-\tau_g/\tau_d \tag{24}$$

which depends on the ratio between the gate time and the decoherence time. Using the parameters given above, we can estimate the ratio τ_g/τ_d. In Table II, it is shown that $\tau_g/\tau_d\approx10^{-2}$ for the two-qubit gate in our scheme and $\tau_g/\tau_d\approx2\times10^{-2}$ for the SWAP operation in the Cirac-Zoller gate at the damping rate $\kappa=4$ MHz. The gate fidelities can thus reach 0.99 with our protocols. This indicates that the Josephson-junction resonator is an effective tool in generating high fidelity quantum operations even at a quality factor $(Q=\omega_c/\kappa)$ of only $Q=7800$ and hence can be used to demonstrate quantum coherence in the TLS fluctuators.

The term $\sigma_{nz}(a+a^\dagger)$ in the residual coupling $\tilde{H}_x$ in Eq. (17) can induce additional decoherence. Here, quantum fluctuations of the resonator mode cause extra noise even at zero resonator amplitude. The spectrum of the quantum fluctuations can be derived as

$$\langle aa^\dagger\rangle_\omega=((\omega-\omega_c)^2+\kappa^2/4)^{-1}\kappa, \tag{25}$$

from which the decoherence rate can be derived as

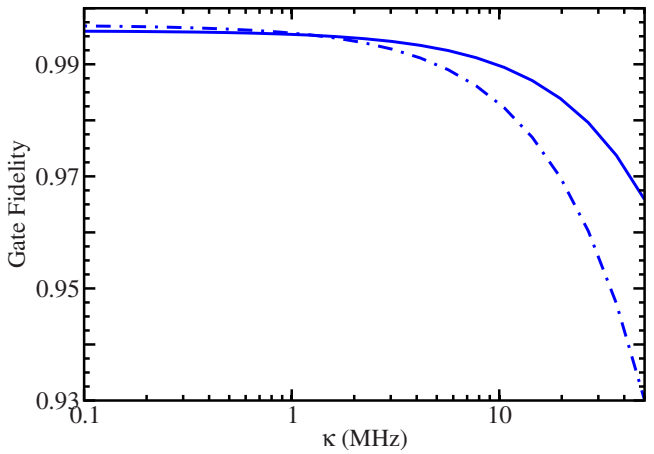

FIG. 3. (Color online) Gate fidelity versus damping rate κ by numerical simulation. Solid curve: SWAP gate and dash-dot curve: Hadamard gate. Two fluctuators are included in the simulation for both gates. For the Hadamard gate, we use the parameters $\Delta_2 = -2\pi \times 80$ MHz and $g_2 = 2\pi \times 30$ MHz for TLS $n=2$.

$$\tau_d^{-1} \sim (\epsilon^2 g_n^4 / \Delta_{nc}^6)\kappa. \tag{26}$$

As can be seen, the decoherence rate is to the fourth order of g_n/Δ_{nc} when the driving amplitude ϵ is comparable with the detunings. With the above parameters, we find that $\tau_d^{-1} \approx 1$ kHz which can be neglected during the gate operations.

To study the effectiveness of the quantum logic gates, we perform numerical simulations on the gate operations using the full Hamiltonian $\tilde{H}_t$. The decay of the resonator is simulated using the Lindblad master equation.[21] This simulation includes both the effect of the residual coupling in Eq. (17) and the effect of the resonator decoherence. We calculate the fidelities of the Hadamard and SWAP gates using the method prescribed by Nielsen's formula for the gate fidelity[25] over a wide range of resonator decay rate. The results are plotted in Fig. 3. This simulation shows that the fidelity can be higher than $F=0.99$ for $\kappa \leq 5$ MHz for single-qubit and two-qubits gates, which also agrees with our estimations above. Hence, at moderate decay rate for the Josephson-junction resonator, high fidelity quantum logic gates can be achieved.

VI. DISCUSSIONS

As demonstrated in recent works, the superconducting resonator can be used to detect the states of qubits or fluctuators.[8,18] In the strong damping regime, the amplitude of the superconducting resonator adiabatically follows the dynamics of the TLS fluctuators, as was shown in our previous work.[18] A phase-sensitive measurement of the resonator can hence provide a direct measurement of the TLS states. In the moderate damping regime where the damping rate is weaker than the coupling constant, a measurement of a TLS can be performed by adjusting the resonator frequency to be in the vicinity of this TLS, but with the condition $g_n \ll |\Delta_{nc}|$. Here, the Stark shift resulting from this TLS is much stronger than that from other qubits. A measurement of the resonances in the transmission spectrum of the resonator can then provide a measurement of the qubit state.[8] Such measurements can be realized with current electronics where the resonator and the driving can be adjusted and switched on and off in nanoseconds, much faster than the decoherence time of the fluctuators.

Our scheme can also be extended to TLS fluctuators inside different junctions. Because the wavelength of the microwave mode of the superconducting resonator is much longer than the dimension of this circuit, fluctuators in different junctions can couple to the same resonator mode when the junctions are connected by a superconducting loop. As is illustrated in Fig. 1(b), two junctions are connected to the central superconducting island labeled by Φ that is associated with the junction resonator. It can be shown that effective coupling between fluctuators in the two junctions can be derived exactly as described by Eq. (11). In this configuration, quantum logic gates can be performed with essentially the same approach as was presented above. This circuit can also be extended to include multiple junctions. This system is thus intrinsically "scalable" where fluctuators in multiple junctions couple nonlocally. Note that the frequency of the superconducting resonator is determined by the total capacitance, the total effective Josephson energy, and the inductance in the circuit, and will decrease as the number of junctions increases. This can set a limit on the number of junctions that can be connected into the circuit.

TLS fluctuators have been studied for a long time. Previously, the fluctuators are often considered as a source of decoherence in superconducting qubits, causing the so-called $1/f$ noise. In this work, we focused on studying the coherent manipulation of the fluctuators which can provide insights about the dynamics, the coupling mechanism, and the relaxation of the fluctuators in superconducting devices. Although the success in implementing universal quantum logic gates makes the TLS fluctuators potential candidate for quantum computing, we want to emphasize that the main aim of this work is to provide a practical scheme to demonstrate the coherence behavior of the fluctuators. Our scheme can be useful for current experiments that investigate the coupling between the fluctuators and superconducting resonators.[3,4,7,15,18,19]

VII. CONCLUSIONS

To conclude, we have shown that universal quantum logic gates can be implemented on spurious TLS fluctuators via the coupling between the fluctuators and the Josephson-junction resonator. Taking into account the full Hamiltonian of the coupled system and the effect of the noise, our numerical simulation of the quantum operations showed that quantum logic gates can be performed with high fidelity even at resonator decay rates of a few megahertz. We have used practical parameters for the junction resonators and the fluctuators in this study. Our work hence indicates that quantum coherence and quantum manipulation of TLS fluctuators can be readily demonstrated. The results here can be generalized to other types of superconducting resonators which are explored in recent experiments.[15]

*ltian@ucmerced.edu
†kjacobs@cs.umb.edu

[1] Y. Makhlin, G. Schön, and A. Shnirman, Rev. Mod. Phys. **73**, 357 (2001); J. Q. You and F. Nori, Phys. Today **58**, 42 (2005); M. H. Devoret and J. M. Martinis, Quantum Inf. Process. **3**, 163 (2004).

[2] P. Dutta and P. M. Horn, Rev. Mod. Phys. **53**, 497 (1981); M. B. Weissman, *ibid.* **60**, 537 (1988); F. C. Wellstood, C. Urbina, and J. Clarke, Appl. Phys. Lett. **85**, 5296 (2004); D. J. Van Harlingen, T. L. Robertson, B. L. T. Plourde, P. A. Reichardt, T. A. Crane, and J. Clarke, Phys. Rev. B **70**, 064517 (2004); O. Astafiev, Y. A. Pashkin, Y. Nakamura, T. Yamamoto, and J. S. Tsai, Phys. Rev. Lett. **96**, 137001 (2006); H. Paik *et al.*, Phys. Rev. B **77**, 214510 (2008).

[3] R. W. Simmonds, K. M. Lang, D. A. Hite, S. Nam, D. P. Pappas, and J. M. Martinis, Phys. Rev. Lett. **93**, 077003 (2004); J. M. Martinis *et al.*, *ibid.* **95**, 210503 (2005).

[4] Z. Kim, V. Zaretskey, Y. Yoon, J. Schneiderman, M. Shaw, P. Echternach, F. Wellstood, and B. Palmer, Phys. Rev. B **78**, 144506 (2008); B. S. Palmer, C. A. Sanchez, A. Naik, M. A. Manheimer, J. F. Schneiderman, P. M. Echternach, and F. C. Wellstood, *ibid.* **76**, 054501 (2007); S. Pottorf, V. Patel, and J. E. Lukens, arXiv:0809.3272 (unpublished); J. A. Schreier *et al.*, Phys. Rev. B **77**, 180502(R) (2008); Y. Yu, S. Zhu, G. Sun, X. Wen, N. Dong, J. Chen, P. Wu, and S. Han, Phys. Rev. Lett. **101**, 157001 (2008).

[5] I. Martin, L. Bulaevskii, and A. Shnirman, Phys. Rev. Lett. **95**, 127002 (2005); A. Shnirman, G. Schön, I. Martin, and Y. Makhlin, *ibid.* **94**, 127002 (2005); R. H. Koch, D. P. DiVincenzo, and J. Clarke, *ibid.* **98**, 267003 (2007); M. Constantin and C. C. Yu, *ibid.* **99**, 207001 (2007).

[6] M. Neeley *et al.*, Nat. Phys. **4**, 523 (2008).

[7] A. M. Zagoskin, S. Ashhab, J. R. Johansson, and F. Nori, Phys. Rev. Lett. **97**, 077001 (2006); S. Ashhab, J. R. Johansson, and F. Nori, N. J. Phys. **8**, 103 (2006).

[8] A. Wallraff *et al.*, Nature (London) **431**, 162 (2004); A. Blais, R. S. Huang, A. Wallraff, S. M. Girvin, and R. J. Schoelkopf, Phys. Rev. A **69**, 062320 (2004).

[9] R. Migliore and A. Messina, Phys. Rev. B **72**, 214508 (2005).

[10] W. D. Oliver *et al.*, Science **310**, 1653 (2005); S. O. Valenzuela *et al.*, *ibid.* **314**, 1589 (2006).

[11] I. Chiorescu *et al.*, Nature (London) **431**, 159 (2004); A. Lupascu *et al.*, Nat. Phys. **3**, 119 (2007).

[12] R. H. Koch, G. A. Keefe, F. P. Milliken, J. R. Rozen, C. C. Tsuei, J. R. Kirtley, and D. P. DiVincenzo, Phys. Rev. Lett. **96**, 127001 (2006).

[13] M. A. Sillanpaa, J. I. Park, and R. W. Simmonds, Nature (London) **449**, 438 (2007).

[14] J. Majer *et al.*, Nature (London) **449**, 443 (2007).

[15] K. D. Osborn, J. A. Strong, A. J. Sirois, and R. W. Simmonds, IEEE Trans. Appl. Supercond. **17**, 166 (2007).

[16] A. A. Houck *et al.*, Nature (London) **449**, 328 (2007).

[17] O. Astafiev *et al.*, Nature (London) **449**, 588 (2007).

[18] L. Tian and R. W. Simmonds, Phys. Rev. Lett. **99**, 137002 (2007).

[19] K. Cicak, M. S. Allman, J. A. Strong, K. D. Osborn, and R. W. Simmonds, arXiv:0810.1976 (unpublished).

[20] T. P. Orlando and K. A. Delin, *Introduction to Applied Superconductivity* (Addison Wesley, Reading, 1991).

[21] D. F. Walls and G. J. Milburn, *Quantum Optics* (Springer, Berlin, 1994).

[22] C. J. Hood *et al.*, Science **287**, 1447 (2000).

[23] A. Blais, J. Gambetta, A. Wallraff, D. I. Schuster, S. M. Girvin, M. H. Devoret, and R. J. Schoelkopf, Phys. Rev. A **75**, 032329 (2007); J. Q. You and F. Nori, Phys. Rev. B **68**, 064509 (2003); O. Gywat, F. Meier, D. Loss, and D. D. Awschalom, *ibid.* **73**, 125336 (2006).

[24] D. Leibfried, R. Blatt, C. Monroe, and D. J. Wineland, Rev. Mod. Phys. **75**, 281 (2003); J. I. Cirac and P. Zoller, Phys. Rev. Lett. **74**, 4091 (1995).

[25] M. A. Nielsen, Phys. Lett. A **303**, 249 (2002).